Rapid Design Process of Shrouded Rotors for Efficient UAV Propulsion

Fabian Chew*, Samuel Gan*, and Henrik Hesse†
University of Glasgow Singapore, 599493 Singapore

A novel approach for the rapid design of unconventional rotor shrouds combining a rapid manufacturing approach with a high-fidelity CFD prediction tool is proposed in this work. Using 3D printing and thrust stand measurements, different shroud designs have been explored experimentally to evaluate the performance gains of propeller shrouds for multirotor vehicles with small-scale, off-the-shelf propellers. The experimental studies are complimented with 3D quasi-steady CFD simulations to gain further insights into the flow fields for unconventional shroud geometries. The framework has been demonstrated for a commercial 5-inch racing-drone propeller, featuring significant performance gains using NACA-shaped shroud profiles.

I. Nomenclature

A	=	Shroud throat cross-sectional area (m^2)	RPM	=	Revolutions per minute (RPM)
A_e	=	Diffuser exit area (m^2)	T	=	Thrust (N)
A_R	=	Rotor disk area (m^2)	T_{Total}	=	Total Thrust (N)
C_P	=	Coefficient of Power (-)	T_{Rotor}	=	Rotor Thrust (N)
C_T	=	Coefficient of Thrust (-)	T_{Shroud}	=	Shroud Thrust (N)
D_t	=	Throat diameter (m)	t	=	Shroud wall thickness (m)
D_e	=	Exit diameter (m)	v_i	=	Induced velocity at rotor plane (m/s)
FM	=	Figure of Merit (-)	w	=	Induced velocity in far wake of rotor (m/s)
FM*	=	Generalised Figure of Merit (-)			
I_d	=	Shroud inlet length (m)	ρ	=	Air density (kg/m^3)
L_d	=	Shroud diffuser length (m)	δ_{tip}	=	Blade tip clearance (m)
n	=	Revolution per second (rev/s)	$\dot{m}$	=	Mass flow rate (kg/s)
P	=	Power generated by the rotor (W)	θ_d	=	Diffuser included angle ($Degree$)
P_i	=	Ideal power (W)	σ_d	=	Expansion ratio (-)

II. Introduction

The application of Unmanned Aerial Vehicles (UAVs) has grown extensively over the last decade from personal toy to various industrial applications, including defense, agriculture, logistics, and inspection. Driving the first commercial uses of UAVs, the logistics sector in particular has seen a lot of momentum in the development of autonomous UAVs as smart delivery solutions. As shown in Fig. 1, major logistics companies such as DHL work towards using drones to tackle the last-mile issue [1]. With the ability to carry heavy payloads over short distances and the lack of a runway requirement, multirotor UAVs are ideal for the operation in urban communities. Another logistics application is the transportation of passengers using eVTOL as the concept by Airbus show in Fig. 1. With the increasing use of multirotor vehicles for such applications, it is likely that we will experience an increased footprint of such systems in urban environments.

---

* Research Student, Aerospace Division (equal contribution to paper)

† Assistant Professor, Aerospace Division, AIAA Member (corresponding author: henrik.hesse@glasgow.ac.uk)

(a) (b)

Fig. 1 (a) DHL Last Mile Parcel Delivery Drone and (b) Airbus eVTOL concept.

This increase in operation, especially in urban settings, comes with the challenges of operating in densely populated areas near buildings and humans which poses a significant danger. Hence, shrouding the propellers as shown in the concept by Airbus in Fig. 1 has been considered as a viable safety measure to protect individuals in the vicinity of the vehicle. As the shroud helps to channel the flow and reduce the propeller tip losses, a well-designed rotor shroud with appropriate shape and tip clearance can also enhance the aerodynamic performance and reduce acoustic footprint [2]. Hence, with improved aerodynamics, rotor shrouding can increase the vehicle electric propulsion efficiency and address the limitation of electric multirotor UAVs in terms of flight duration due to the limited battery capacity. To design an efficient shroud, however, several design parameters including shroud and propeller geometry need to be considered [3, 4]. This project therefore works towards a novel design process combining aerodynamic analysis of shrouded rotors through Computational Fluid Dynamics (CFD) and rapid prototyping for experimental validation.

In fact, the benefits of rotor shrouding have been exploited since the onset of rotor-based flight in 1950s. Experimental studies on small-scale rotors (or ducts) in 1958 already demonstrated the benefits of shrouds and analyzed the increase in static thrust with increasing shroud exit area [5]. The reviews by [6] and [7] provide an in-depth overview of the developments from the early experiments on large-scale vehicles all the way to very small Micro Aerial Vehicles (MAVs) [7]. All studies consistently conclude that shrouding improves the aerodynamic efficiency of the rotor compared to the open rotor configuration. However, with propeller shrouding increasingly applied to a range of multirotor configurations from very small scale [8], [9] to larger eVTOL rotors, such as the example by Airbus shown in Fig. 1, it is critical to understand how the efficiency of the shrouded rotor is driven by the rotor geometry and shroud shape. Early work focused on understanding the effects of rotor configuration on the aerodynamic performance, and more recent studies analyzed the effect of the shroud shape, such as shroud profile and shroud chord-diameter ratio [2].

Recent studies [10] found that, in addition to tip clearance, a major contribution to the shroud performance lies in the shroud profile diffuser angle and the overall shroud profile [11]. With a higher expansion ratio, the total thrust can be increased, but it is critical that the shroud profile allows the flow to expand smoothly to avoid flow separation. The behavior is similar to flow over a conventional airfoil typically designed using smooth NACA profiles. Hence, Yilmaz et al [2] experimentally investigated five different shroud shapes using different NACA airfoil profiles for the shroud. The study focused on VTOL UAVS and analyzed takeoff and forward flight modes. In hover conditions, the shrouded rotors outperformed the open rotor configuration where the NACA7312 profile provided the best performance. However, with increasing advance ratios, the experiments showed that the thrust obtained from the shrouded configurations decreases, making the shroud unfavorable at high freestream velocities, such as forward flight modes.

With the availability of higher fidelity CFD simulations over the last decades it has become feasible to analyze the aerodynamic performance of shrouded rotors numerically. Using a quasi-steady CFD approach allows relatively fast predictions of propeller aerodynamics based on a Multiple Reference Frame (MRF) model. Kutty et al [12] used the MRF approach with a standard k-ω turbulence model to analyze the aerodynamics of an off-the-shelf APC 10x7 inch propeller. Comparison to experimental wind-tunnel data of open rotors for a range of advance ratios, from 0.192 to 0.799 showed good comparison with only a slight underprediction of the power coefficient at low advance ratios, and an over prediction for higher advance ratios. The additional weight of the shroud is a major disadvantage of shrouded rotor systems as the aerodynamic benefit is penalized by the additional thrust requirement to carry the shrouds. Kuantama et al [13] demonstrated the use of CFD to analyze shrouded and open rotor configurations. The study

compared different shroud geometries with the aim to minimize the total weight of the shroud. Another way to increase the overall thrust output for each rotor is the use of counterrotating coaxial rotors which is often featured in heavy-lift designs such as the concepts shown in Fig. 1. Xu [14] analyzed the effects of propeller spacing and pitch angle for a shrouded twin counterrotating propeller system through steady-state CFD simulation and using the k-ω Shear Stress Transport (SST) model. For shrouded counterrotating propellers, such as the Airbus concept in Fig. 1, the total thrust for the system is highly dependent on the ratio of spacing between propellers to the propeller diameter and blade pitch angle [15]. The presence of a shroud does not always improve the thrust performance in a shrouded co-axial rotor system [14].

It is clear that there are aerodynamic benefits to rotor shrouding in addition to the safety feature. However, with the increasing use of shrouding for UAVs, it is critical that designers understand the effects of the shroud geometry and its interaction with the propeller geometry to obtain any gains from shrouding. Hence, this work proposes a design methodology for the rapid development of rotor shrouds. The proposed rapid design process combines CFD analyses of potential shroud geometries with a rapid prototyping approach and thrust testing for instant experimental validation. Different shroud designs can be quickly evaluated to compare the aerodynamic performance of shrouded rotors to arrive at an optimal rotor configuration for a specific UAV design. In this paper we specifically analyze shroud designs based on NACA profiles [2] but focusing on small-scale rotors with diameters of 5-8 inches.

Most drone concepts currently sprouting all over the world further rely on off-the-shelf propellers, even for eVTOL concepts with propellers as large as 40 inches. With the framework developed in this work, we can quickly evaluate the benefits of shrouding the rotors using off-the-shelf propellers by evaluating the aerodynamic gains against the resulting weight penalties. Even if shrouds are used as a critical safety feature, such as propeller guards, the proposed analysis tool can provide predictions on rotor performance and interactions with the vehicle frame, to optimize the propeller guards to provide additional aerodynamic benefits.

III. Rapid Design Process for Rotor Shroud Evaluation

Open rotors produce significant vortices at the propeller tips which can interact with the surrounding structure. The resulting turbulence leads to loss in aerodynamic efficiency and can have detrimental effects on the vehicle stability. By encapsulating the rotors, shrouded designs prevent the vortices from propagating which also prevents interaction of the vortices with the vehicle frame. This leads to greater thrust produced by the shrouded configuration compared to an open rotor design of the same diameter and power loading. The performance of shrouded rotors, however, heavily depends on the shroud geometry and the key parameters defined in Fig. 2. The schematic also illustrates the conventional shroud design which typically consists of a straight inlet and an angled diffuser. This conventional shrouded rotor (SR) is simple to manufacture and numerous studies over the last decades have evaluated the effects of the key parameters on the shroud performance demonstrating the increased efficiency compared to open rotor (OR) equivalents.

However, the conventional designs can lead to suboptimal flow transition, especially at the sharp edge from inlet to diffuser, and recent studies have explored the use of more streamlined shroud geometries using cambered airfoil profiles. Experimental investigation by Yilmaz et al [2] of five different NACA-based shroud profiles found that the highly cambered NACA 7312 configuration provides the best overall performance. The illustration in Fig. 3 depicts the differences between a NACA 7312 profile and the conventional shroud design.

Despite the obvious advantages of unconventional NACA-based shroud configurations, the complex shape of these geometries makes it more difficult to manufacture which typically requires a mold. Hence, if a UAV designer wants to equip the vehicle with such a complex NACA-based shroud geometry, a reliable prediction tool is required to evaluate the aerodynamic performance before a mold is manufactured. In this work we therefore propose a design process making use of rapid prototyping to generate complex shroud geometries for small-scale, off-the-shelf propellers. The experimental results from thrust stand measurements are compared against validated CFD results which will ultimately serve as a prediction tool for the shroud design analysis.

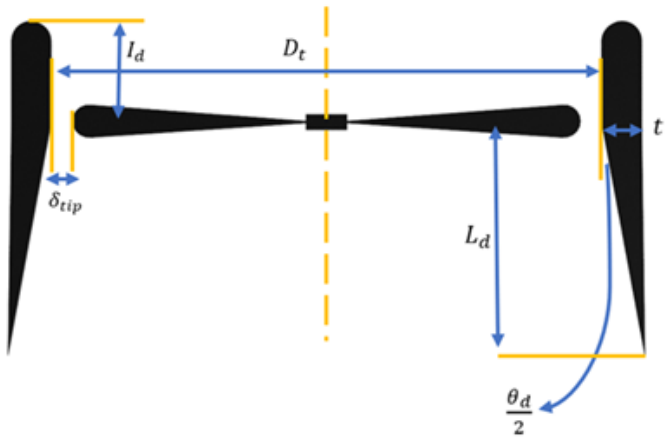

Fig. 2 Key parameters for conventional shroud geometry: throat diameter (D_t), inlet length (l_d), diffuser length (L_d), shroud thickness (t), blade tip clearance (δ_{tip}), and diffuser included angle (θ_d).

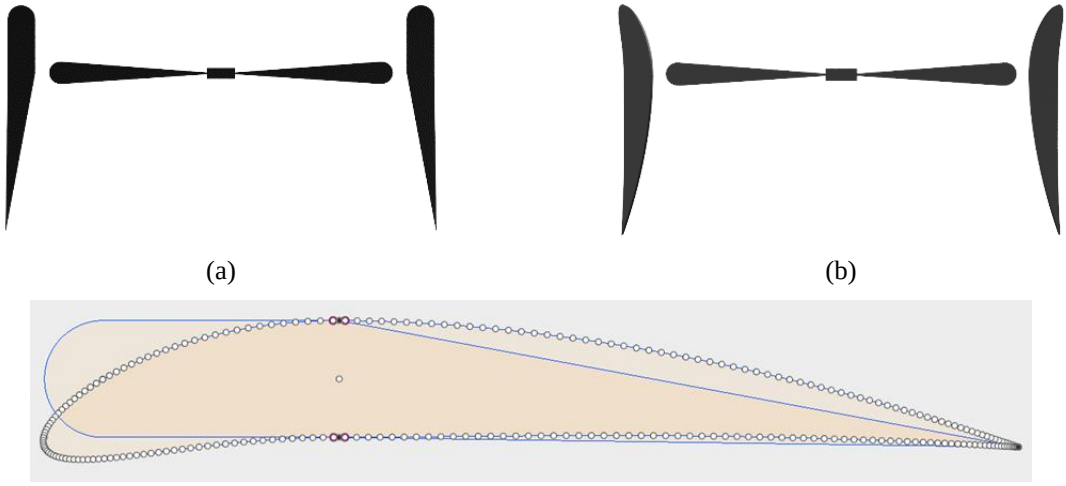

Fig. 3 Shroud geometries with (a) conventional, (b) NACA 7312 shroud, and (c) comparing both profiles.

A. Propeller Theory

To compare the rotor performance for the different diameters and shroud configurations, we will extensively use the coefficients of thrust C_T and power C_P in this work and will define these briefly here for open and shrouded rotor configurations. For an open rotor, we can predict the aerodynamic coefficients in terms of propeller rotational speed n, diameter D, thrust T, and power P as [7],

$$C_T = \frac{T}{\rho n^2 D^4} \text{ and } C_P = \frac{P}{\rho n^3 D^5} \tag{1}$$

with air density ρ. Further considering the freestream velocity V and the advance ratio J, relating freestream fluid to the propeller tip speed as,

$$J = \frac{V}{nD} \tag{2}$$

we can compute the efficiency of the propeller η as,

$$\eta = \frac{C_T J}{C_P} = \frac{TV}{P} \tag{3}$$

For a shrouded propeller, we need to consider the contribution of propellers and the shroud to the total thrust,

$$T_{total} = T_{rotor} + T_{shroud} \tag{4}$$

which is used to calculate the thrust coefficient and efficiency for the shrouded rotor using Eqs. (1-3). From simple momentum theory we can estimate the total thrust T_{total} as,

$$T_{total} = \dot{m}w \tag{5}$$

where w is the far wake axial velocity and $\dot{m}$ is the mass flow rate, which can be estimated as,

$$\dot{m} = \rho A_e w \tag{6}$$

with the far wake area assumed as $A_e = 0.5A$ for an open rotor configuration.

The Figure of Merit (FM) is typically used to evaluate the static thrust efficiency of rotors and is defined as the ratio of the ideal power P_i to the actual amount of power P by a propeller to produce a given thrust, i.e. $FM = P_i/P$. The ideal power P_i can be found as

$$P_i = \frac{T^{3/2}}{\sqrt{4\sigma_d \rho A}} \tag{6}$$

where the expansion ratio σ_d is

$$\sigma_d = \frac{A_e}{A} \tag{7}$$

which can be predicted as 0.5 for open rotor configurations using simple momentum theory. For a shrouded rotor, the expansion ratio is the shroud exit area A_e over the throat area A_t as defined in Fig. 2.

However, due to the different expansion ratios, the FM cannot be used to compare between open and shrouded rotors. Hence, Pereira [7] introduced the generalized Figure of Merit FM^* as,

$$FM^* = FM\sqrt{\sigma_d} \tag{8}$$

which is independent of the expansion ratio and hence can be used to compare between open and shrouded propellers. Using FM^* we can then compute the power loading of the rotor which relates the thrust produced by the rotor to the power required to produce that thrust, i.e.

$$\frac{T}{P} = \sqrt{\frac{4\rho A_t}{T}} \cdot FM^* \tag{9}$$

Using the definition of the thrust loading above we can finally compute the thrust at a fixed power as,

$$T = \left(\sqrt{4\rho A_t} \cdot FM^*\right)^{2/3} \cdot P \tag{10}$$

or, alternatively, find the power at a fixed thrust output as,

$$P = \left(\frac{1}{\sqrt{4\rho A_t} \cdot FM^*}\right) \cdot T^{3/2} \tag{11}$$

The simple propeller theory presented here will be used to compare the aerodynamic performance of different shroud configurations following the experimentation framework presented next.

B. Rapid Prototyping for Aerodynamic Analysis of Shroud Designs

In this work we propose a novel approach for rapid design of different shroud configurations. The method is tailored towards small-scale UAV systems using off-the-shelf propellers. From the different forms of rapid prototyping, fused deposition modeling or 3D printing is used in this work. 3D printing has the advantage that we can quickly produce arbitrary shroud geometries at low cost. The disadvantage of 3D printing shroud shapes for performance testing, however, is the low heat resistance of the material and the comparatively poor surface finishing. In this case we used Polylactic Acid (PLA) filament and could easily polish the parts after the different shroud geometries were printed.

The performance of the different rotor configurations was compared using the RCBenchmark Thrust Stand Dynamometer 1580 Series [16] as shown in Fig. 4. The thrust stand can test rotors producing up to 50 N thrust and 1.5 Nm torque. It records the instantaneous thrust using a load cell, the propeller speed and the power consumed by the entire system. An anemometer was used to evaluate the exit velocities of the rotor. While the thrust stand can

measure the rotor thrust directly, for the shrouded designs we need to consider the total thrust which constitutes of the thrust generated by the rotor and shroud as defined in Eq. (4). We estimate this total thrust output of the shrouded designs from conservation of momentum Eq. (5) using the exit velocity measurements.

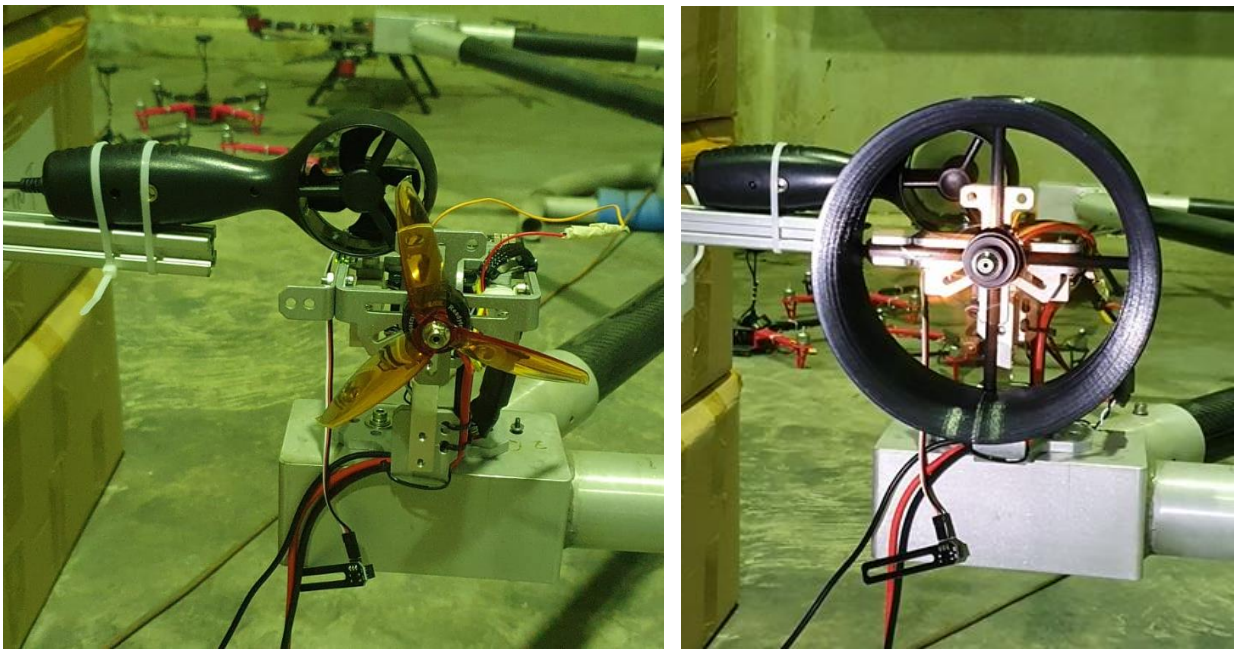

(a) (b)

Fig. 4 Thrust stand setup with (a) open rotor and (b) 3D printed NACA 7312 shroud.

In this work we demonstrate the proposed method for two different experiments to (i) compare the performance benefits of a NACA-shaped shroud over conventional designs, and (ii) perform a full performance analysis for a small-scale, 3-bladed ducted propeller. The latter will be used to compare against CFD results.

1. Experimental Analysis of Optimized Shroud Design

In this study, three different configurations have been analyzed to demonstrate the rapid design approach by comparing the open rotor configuration with the two shrouded configurations using the NACA-based shroud design (NACA 7312) and a conventional shroud configuration with a straight throat and angled diffuser as shown in Fig. 5. We will use the experimental results to demonstrate the advantage of a NACA-shaped shroud over the conventional shroud design as proposed by Yilmaz et al [2]. Both designs have exact same tip clearance, inlet length, diffuser length, and exit area as defined in Table 1.

Table 1 Comparison of key parameters for conventional and NACA 7312 shroud geometries for parameters defined in Fig. 2.

Shroud key parameters	Typical Shroud (SR)	NACA 7312 Shroud (NACA)
Throat diameter, D_t	165 mm	165 mm
Exit Diameter, D_e	191 mm	191 mm
Shroud thickness at rotor point, t	12 mm	12 mm
Inlet length, I_d	30.25 mm	N/A
Diffuser length, L_d	69.75 mm	N/A
Diffuser included angle, $\theta_d/2$	10.6 deg	N/A
Propeller tip clearance, δ_{tip}	6.3 mm	6.3 mm

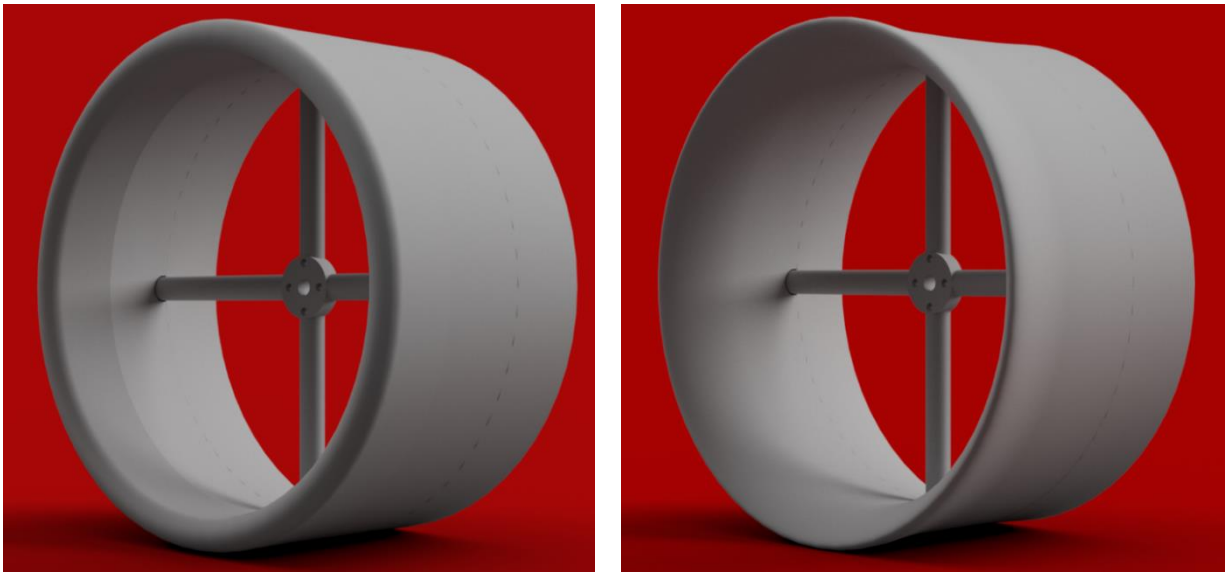

(a) (b)

Fig. 5 CAD design of (a) conventional shroud and (b) NACA 7312 shroud.

To compare the performance of the open rotor (OR), conventional shrouded rotor (SR), and NACA shroud (NACA), we have tested 10 different propellers at three different rotation speeds of 3,000, 4,000, and 5,000 RPM. As shown in Table 2, all propellers are 6 inches in diameter but vary in shape, pitch, and materials. In all experiments we replicate a hovering condition with zero inflow velocity.

Table 2 Overview of 6-inch propellers.

Propeller Configuration	Propeller Material	Pitch (inches)	Propeller Diameter (inches)
1	Wood	5	6
2	Plastic	4.5	6
3	Composite Plastic	4	6
4	Polycarbonate	5	6
5	Polycarbonate	4	6
6	Carbon Fibre	4.5	6
7	Carbon Fibre	4.5	6
8	Carbon Fibre	4	6
9	Plastic	4	6
10	Plastic	3	6

Naturally the 10 different propeller geometries have different performance characteristics. Hence, over 100 different experiments were conducted to draw statistics of the rotor performance for the different propellers and shroud configurations as presented in Fig. 6. In this case the power input to the rotor has been fixed and the obtained thrust is compared for all cases.

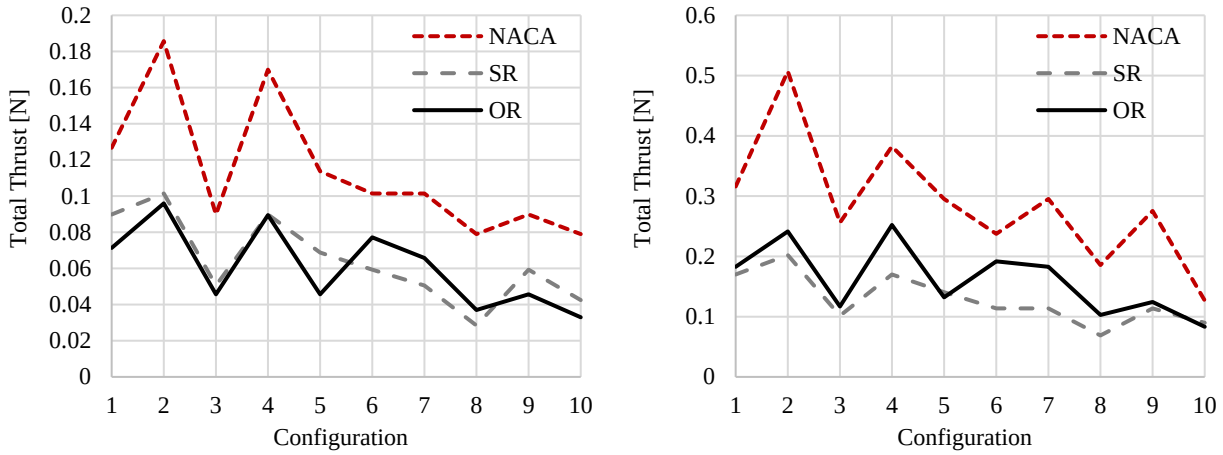

Fig. 6 Rotor performance at constant input power comparing thrust of shrouded designs against open rotor (OR) for (a) 3,000 RPM and (b) 5,000 RPM for the 10 configurations defined in Table 2.

The statistics in Fig. 7 compare the performance of the NACA-based shroud against the conventional shroud in terms of percentage difference to the open rotor performance. The results for 3,000 RPM show that the NACA-based design can produce 2.5 times the thrust compared to the open rotor for a specific propeller design while all propellers in average produce almost twice the amount of thrust compared to the OR configuration. This performance increase is superior to the conventional shroud which increases the thrust to 1.5 times of the open rotor configuration for the best propeller configuration with an average increase of 1.1 times. These results are consistent with findings by Yilmaz et al [2] which also showed the best performance for the NACA-based shroud using the NACA 7312 profile. We can draw further conclusions for 5,000 RPM that a conventional shroud can even deteriorate the thrust output for high RPM for specific propeller configurations.

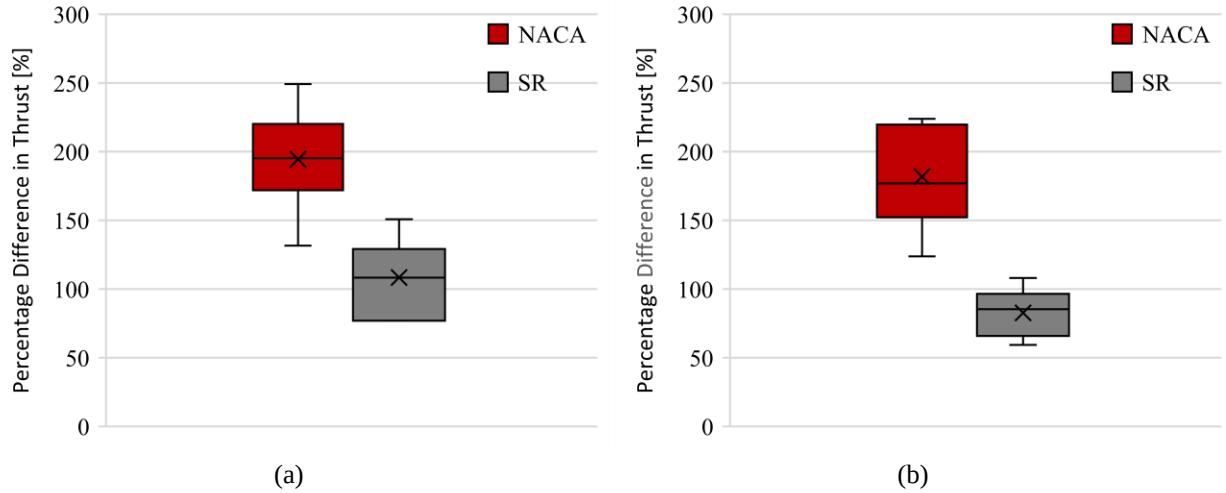

Fig. 7 Rotor performance statistics comparing the percentage difference of shrouded designs against open rotor configurations for the 10 configurations shown in Fig. 6 for (a) 3,000 RPM and (b) 5,000 RPM.

2. Performance Analysis of Optimal Shroud Design for 3-Bladed Propeller (Gemfan 5152 Flash)

In this study we experimentally investigate a shroud design for a 3-bladed Gemfan propeller as illustrated in Fig. 8. The Gemfan 5152 Flash is a popular racing drone propeller with 5-inch diameter and optimal performance at high propeller speeds of up to 10,000 RPM. The CAD geometry for this propeller is readily available and will also serve as comparison against CFD results in Section IV.B for the open rotor and shrouded configurations. Following the comparison of shroud designs in Section III.B.1, in this section we limit the analysis to a NACA-shaped shroud using

a NACA 7312 profile. The shroud design is also illustrated in Fig. 8 (right) with the shroud parameters defined in Table 3. For the experimental study we only considered a tip clearance of 0.6% but the other tip clearance cases have been considered in CFD as presented in Section IV.B. For the experimental study we again use the RCBenchmark Thrust Stand Dynamometer 1580 Series [16] as shown in Fig. 4 for the Gemfan propeller and 3D printed shroud design. To obtain consistent results for all rotor speeds and configurations, an external power supply (as opposed to Li-Po battery) was used to deliver a constant voltage.

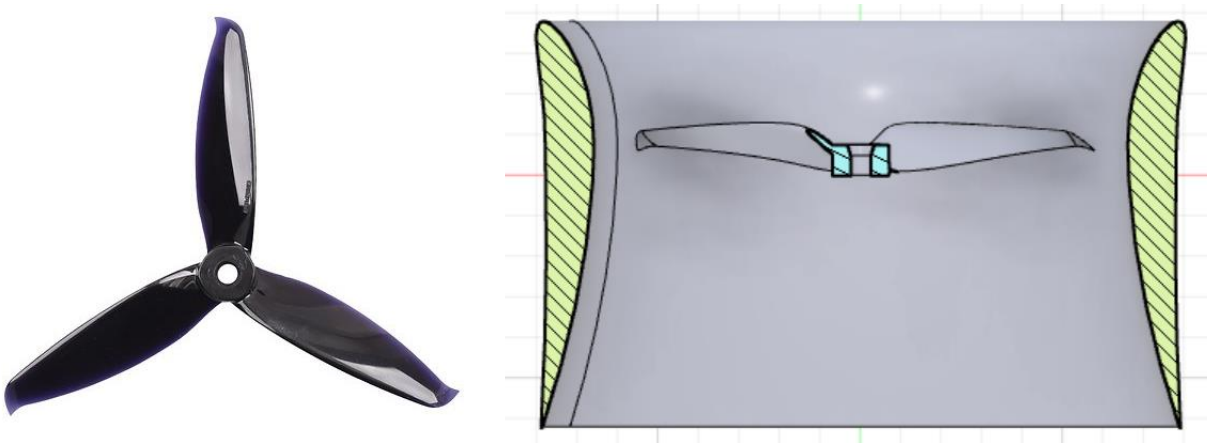

(a) (b)

Fig. 8 (a) Gemfan 5152 Flash propeller with 5-inch diameter. (b) NACA 7312 shroud design with 0.6% tip clearance as defined in Table 3.

Table 3 Parameters for NACA 7312 shroud for the 5-inch Gemfan propeller shown in Fig. 8.

Shroud key parameters	**0.6% Tip Clearance**	**1.11% Tip Clearance**	**3.57% Tip Clearance**
Exit Diameter, D_e	0.158 m	0.160 m	0.166 m
Throat diameter, D_t	0.132 m	0.133 m	0.140 m
Shroud throat area	0.0137 m^2	0.0140 m^2	0.0153 m^2
Propeller disk area A_r	0.0127 m^2	0.0127 m^2	0.0127 m^2
Shroud exit area A_e	0.0197 m^2	0.0200 m^2	0.0216 m^2
Expansion ratio, σ_d	1.44	1.43	1.41
Diffuser length, L_d	0.6975 m	0.6975 m	0.6975 m
Inlet length, I_d	0.3025 m	0.3025 m	0.3025 m
Propeller Model	Gemfan 5152 Flash	Gemfan 5152 Flash	Gemfan 5152 Flash

The thrust stand results in Fig. 9 compare the total thrust and power for the NACA-based design (NACA) against the open rotor (OR) configuration. Similar to the experimental results above, we can observe again that the shrouded design increases the total thrust significantly over the entire range of propeller speeds. The maximum increase is observed at 8,000 RPM of 2.8 times the open rotor thrust output. However, this improvement in total thrust is not driven by an increase in power as compared in Fig. 9 (b). Both designs require comparable power over the range of analyzed propeller speeds.

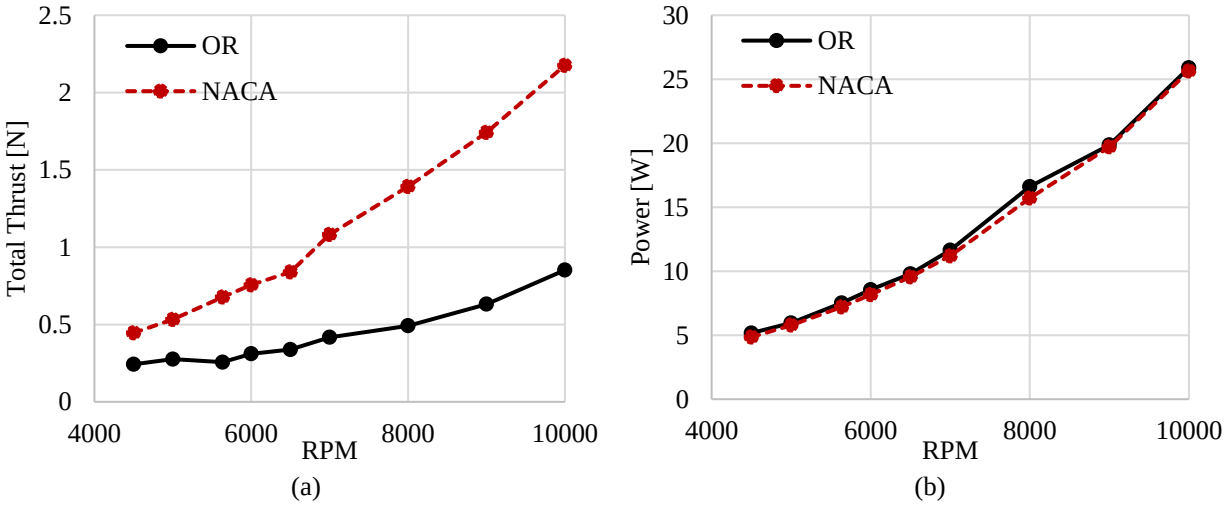

Fig. 9 Comparison of rotor performance for Gemfan 5152 Flash propeller of NACA-based shroud design (NACA) against open rotor (OR) configuration: (a) total thrust, (b) power.

Hence, the shroud design is able to produce considerably more thrust without additional power detriment. This is also reflected in the results shown in Fig. 10 (a) which compare the power required per unit thrust for shrouded and open rotor configurations. Using the generalized Figure of Merit FM^* as defined in Eq. (8), we can further compare the static thrust efficiency of the shrouded design against the open rotor configuration. As expected from the reduced power requirements for the shroud design, the FM^* significantly improves using the shroud configuration as shown in Fig. 10 (b). The experimental results further show that the FM^* for the shrouded configuration improves even further at higher propeller speeds while the open rotor FM^* follows the expected trend of a constant performance for the entire RPM range. The Gemfan 5152 Flash propeller is designed for racing drones running at high propeller speeds. Hence, the superior performance at high RPM is expected, but the results show that the shroud can significantly improve aerodynamic performance of the propellers at their ideal operating range. The underlying physical effects which may cause this trend will be analyzed next using the CFD environment for propeller analysis.

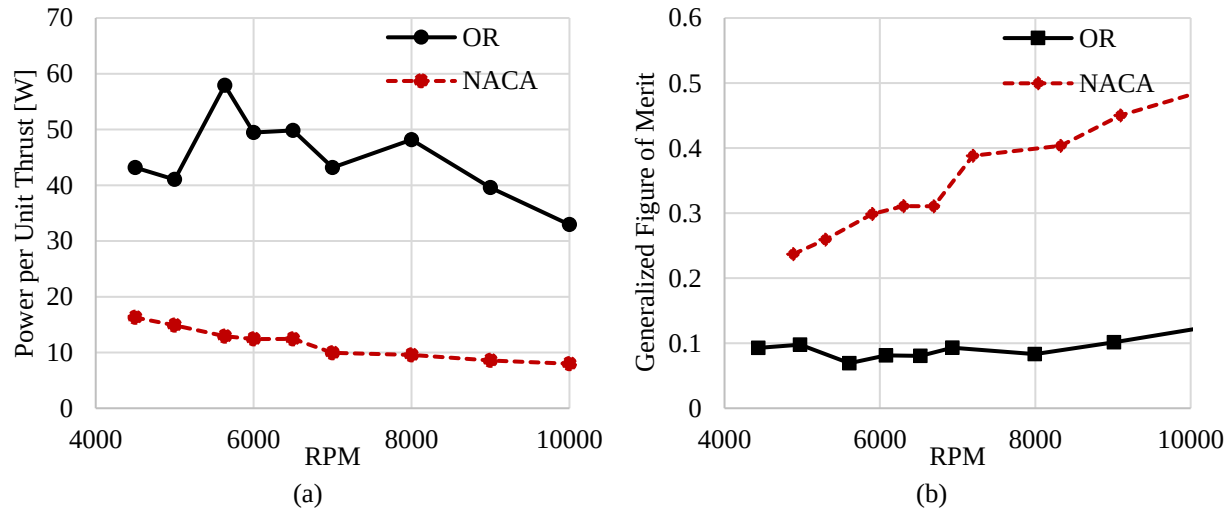

Fig. 10 Comparison of rotor performance for Gemfan 5152 Flash propeller of shroud design (NACA) against open rotor (OR) configuration with (a) power per unit thrust and (b) generalized Figure of Merit.

IV. CFD Framework for Rotor Shroud Optimization

To complement the rapid design approach introduced in Section III, this work further considers a simulation approach to evaluate the aerodynamic performance of shrouded rotors. The CFD environment can be used as a fast prediction tool for novel shroud geometries and to explore detailed flow features inside the rotor to further improve designs. In this work, we use ANSYS Fluent to simulate the shrouded rotor in 3D using a RANS approach with an SST k-ω turbulence model [17]. The overall methodology for the simulation methodology is summarized in Fig. 11 and includes the general steps of domain setup, boundary conditions, solver selection, mesh convergence analysis, and analysis.

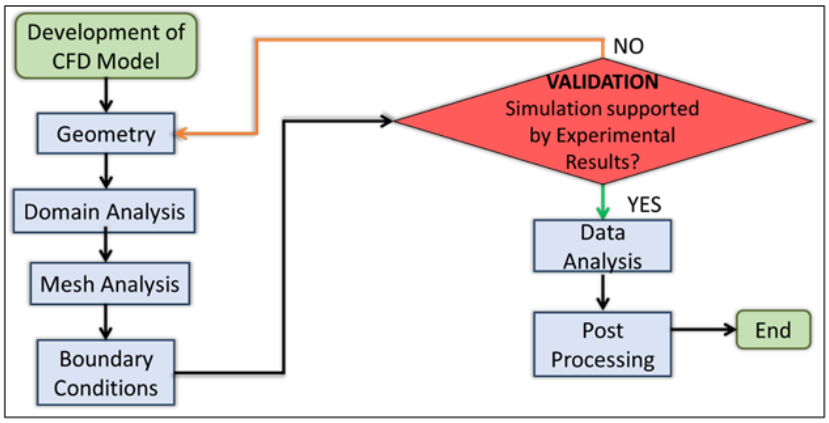

Fig. 11 Overview of CFD approach for propeller simulation.

Following the propeller analysis in [12], this work also uses the MRF approach to model the rotating rotor through a steady-state approximation where individual cell zones can have different rotational or translational velocities [17]. As shown in Fig. 12, the problem is set up as two main domains which constitute the rotating domain and the stationary domain. The propeller is located inside the rotating domain and a rotational speed of the propeller is defined. The shroud on the other hand is in the stationary domain which has no rotational component and represents the ambient condition or wind tunnel environment. A freestream velocity for the stationary domain can be defined to reproduce environmental conditions. A domain convergence study by Xu [14] for shrouded rotors suggests that a minimal stationary domain diameter of 11 times the diameter of the propeller, an upstream length of 9 times the diameter, and a downstream length of 11 times the propeller diameter is required to accurately capture the propeller wash. The domain boundaries have also been illustrated in Fig. 12. Note that the rotating domain size is slightly larger than the diameter of the propeller to ensure that the entire propeller is fully encapsulated in the rotating domain, however, without coming into contact with the shroud.

A. Validation of Open Rotor and Shrouded Rotor Analysis

A crucial consideration in the proposed use of CFD as a rapid design tool for propeller shrouding is the expected accuracy of the results. We therefore first provide an overview of the validation studies for the open rotor and shrouded configurations. The open rotor results have been validated against wind tunnel results by Brandt and Selig [18] for an off-the-shelf APC 8 x 3.8" clockwise-rotating propeller with the CAD model shown in Fig. 13 (a).

Following the proposed CFD approach at sea-level reference conditions of 4,007 RPM and 2.958 m/s inlet velocity (advance ratio of 0.218), we obtain the convergence results in Table 4. A refinement of the propeller surface as shown in Fig. 13 (b) is required to obtain the performance predictions of $C_T = 0.076$, $C_P = 0.0398$, and $\eta = 0.418$ for the converged case which are very close to the wind tunnel results with relative errors of 0.72%, 0.67%, and 0.26%, respectively. This initial validation study for an open rotor configuration highlights the strength of the steady-state CFD approximation to provide extremely accurate rotor predictions at acceptable computation times.

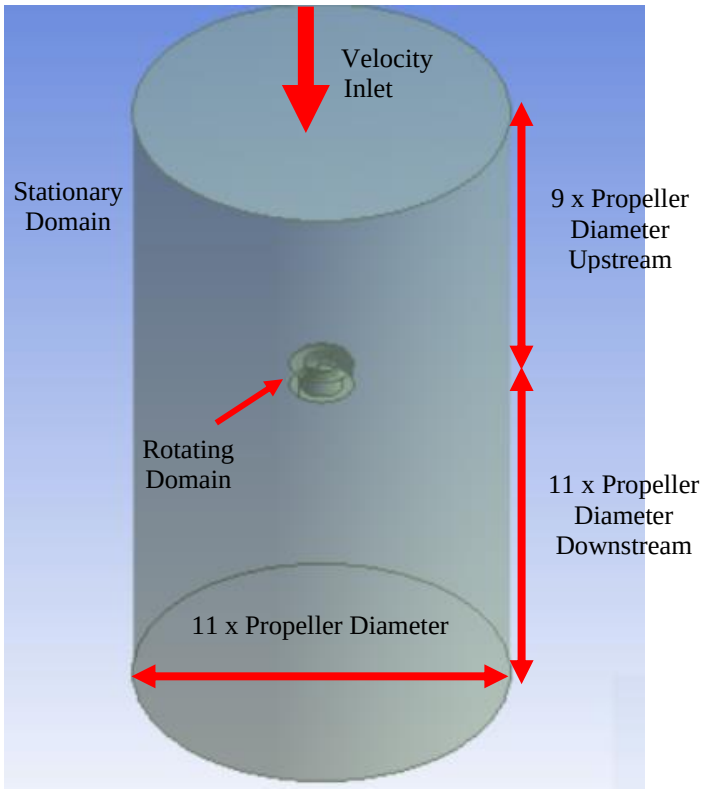

Fig. 12 Domain and boundary setup for shrouded propeller.

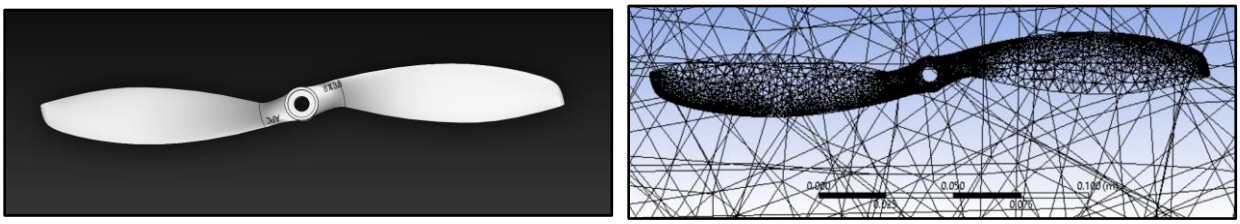

(a) (b)

Fig. 13 (a) CAD Model and (b) 'Fine' mesh size for APC 8x3.8" Propeller.

Table 4 Mesh convergence and validation results for open rotor CFD analysis with APC 8x3.8" Propeller.

Mesh	Number of Elements	CFD Results		Wind Tunnel data [18]		Percentage Deviation	
		C_T	C_P	C_T	C_P	C_T	C_P
Coarse	145,990	0.0711	0.0384	0.0771	0.0401	-7.82%	-4.30%
Medium	303,600	0.0722	0.0390	0.0771	0.0401	-6.36%	-2.67%
Fine	583,906	0.0785	0.0409	0.0771	0.0401	1.79%	2.08%
Refinement	**1,798,510**	**0.0765**	**0.0398**	**0.0771**	**0.0401**	**-0.72%**	**-0.67%**

To further validate the CFD approach for shrouded rotors, we compare against the experimental data by Pereira [7] evaluating the performance of MAVs affected by varying the shroud profile shapes. In hover conditions, a rotor collective angle of 20 degrees was chosen, rotating over a range of 1,000 to 2,500 RPM, paired with a shroud model of $LR09 - D20 - \delta 0.5$. The shroud has a shroud throat diameter of $D_t = 159$ mm, shroud inlet lip radius of $r_{lip} = 14.31$ mm, diffuser included angle of $\theta_d = 20$ deg, blade tip clearance of $\delta_{tip} = 0.795$ mm, and a shroud diffuser

length of $L_d = 114.48$ mm. Comparison of the modeled shroud against the original definition by Pereira [7] can be seen in Fig. 14. The resulting 3-bladed configuration of the whole experimental system is compared in Fig. 15 against the CFD implementation.

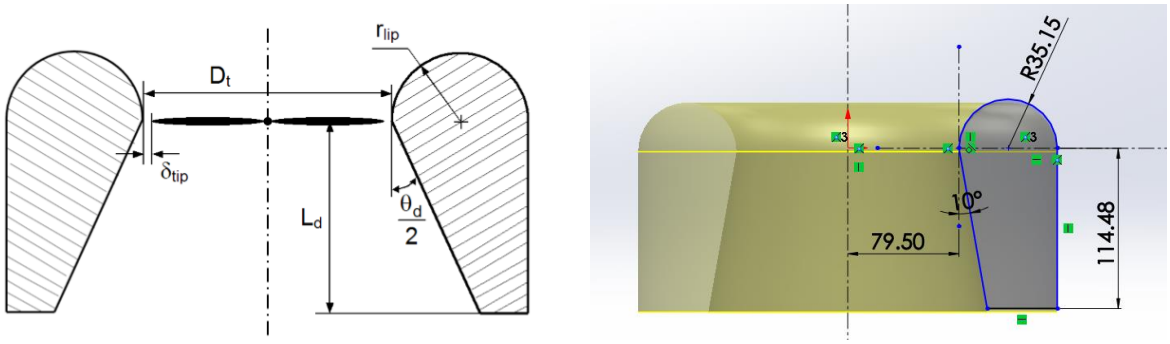

(a) (b)

Fig. 14 Definition of shroud geometry (a) by Pereira [7] and (b) CFD model.

The comparison of the CFD results for the shrouded rotor against experimental results in Table 5 for zero inflow and 2,000 RPM shows very good agreement between the CFD and experimental results. The same agreement can be observed for other rotational velocities and advance ratios. Hence, the demonstrated CFD implementation using the MRF approach provides a reliable prediction tool for shrouded rotor analyses with relative errors as low as 4% in thrust and power predictions. The CFD environment further provides insights into the flow characteristics as illustrated in Fig. 16 for this validation case at two different propeller speeds.

(a) (b)

Fig. 15 (a) Experimental system by Pereira [7] compared with (b) CAD representation of shrouded rotor.

Table 5 Mesh Convergence and validation results against experimental results in [7] for 2000 RPM and zero inflow.

Mesh	Number of Elements	CFD		Experiment [7]		Percentage Deviation	
		C_T	C_P	C_T	C_P	C_T	C_P
Coarse	452,256	0.0182	0.00325	0.019	0.004	4.04%	18.67%
Medium	959,317	0.0184	0.00342	0.019	0.004	3.28%	14.61%
Fine	**1,612,091**	**0.0194**	**0.00383**	**0.019**	**0.004**	**2.03%**	**4.32%**
Refinement	3597640	0.0194	0.00378	0.019	0.004	2.15%	-5.59%

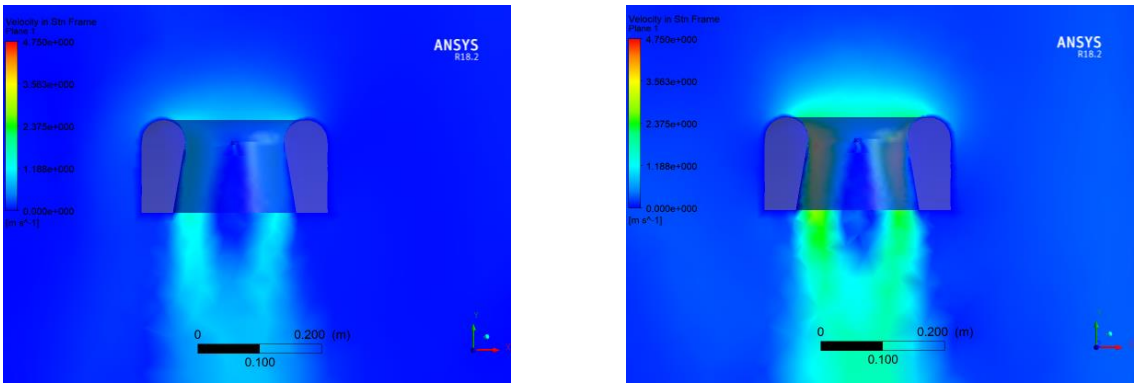

(a) (b)

Fig. 16 Velocity in stationary frame of shrouded propeller in [7] for (a) 1,000 and (b) 2,000 RPM.

B. CFD Analysis of NACA-Shaped Shroud Design with 3-Bladed Propeller (Gemfan 5152 Flash)

The CFD environment has been used next to evaluate the performance gains of the NACA-based shroud design with the 3-bladed Gemfan 5152 Flash propeller. The results in this section will be used to compare against the corresponding experimental results in Section III.B.2 and gain further physical insights into the flow characteristics for different tip clearances of 0.6%, 1.1% and 3.6%. As a result of considering the different tip clearances for the shroud (keeping the propeller size fixed), Table 3 also shows the overall profile parameters for the different shrouds that have been used in this study. Similar to the experimental study presented in Section III.B.2, we also consider the NACA 7312 shroud profile as shown in Fig. 8 (b). The different tip clearances considered here follow reference values from ducted marine propellers in [19] and will be used to study the effect of tip clearance on performance gains of shrouded designs.

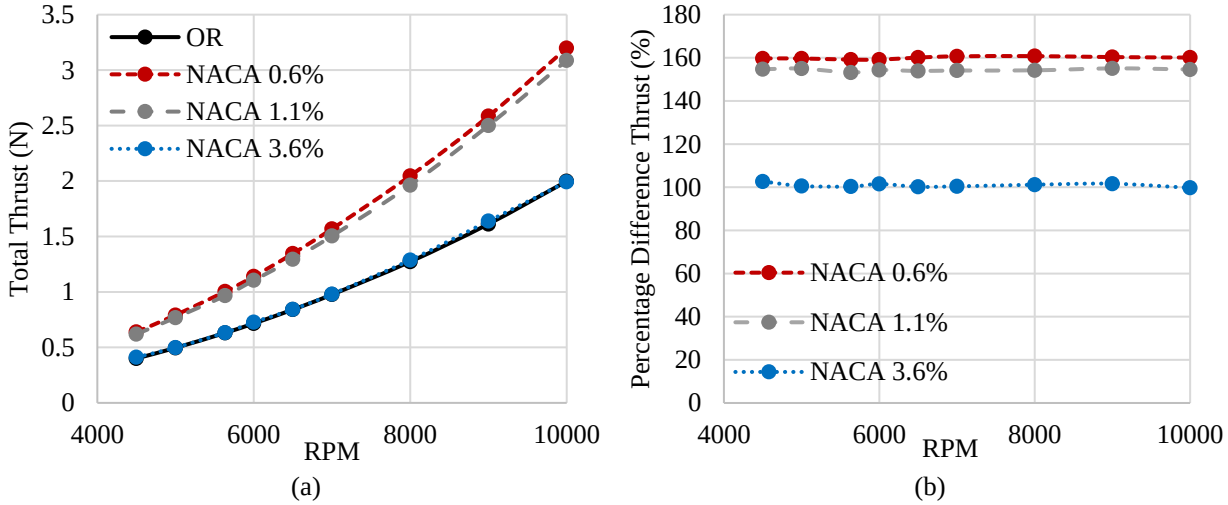

(a) (b)

Fig. 17 (a) Comparison of total thrust for Gemfan 5152 Flash propeller with NACA-based shroud design (NACA) against open rotor (OR) configuration. The NACA shrouds include different tip clearances of 0.6%, 1.1%, and 3.6%. (b) Rotor performance statistics comparing the percentage difference of shrouded designs against open rotor configurations for different tip clearance.

CFD simulations for the open rotor and NACA shroud configurations were conducted in simulated hover condition with no inflow into the rotor but at different rotational speeds between 4,500 and 10,000 RPM which represent the test conditions for the experimental results in Section III.B.2. The results in Fig. 17 and Fig. 18 demonstrate the benefits of using rotor shrouds with the NACA shroud design producing higher thrust values compared to the open rotor configuration across the range of propeller speeds considered. However, we note the importance of considering the tip clearance. While the tip clearances of 0.6% and 1.1% produce comparable results, a sudden drop in performance can be observed for 3.6% tip clearance. This highlights the importance of achieving fine manufacturing tolerances, as

large tip clearances reverse the performance gains of the propeller shroud while adding additional weight. From the total power predictions in Fig. 18 (a) we observe that all shroud designs have similar power requirements compared to the open rotor configuration. Hence, with the increase in total thrust output for a comparable power, the CFD results also confirm the improvement in overall propulsion performance of shrouded propellers. However, the predicted generalized FM^* values in Fig. 18 (b) further demonstrates the importance of low tip clearances to achieve the desired increase in FM^* from close to 30% for the open rotor to over 60% for the shrouded configuration with 0.6% clearance.

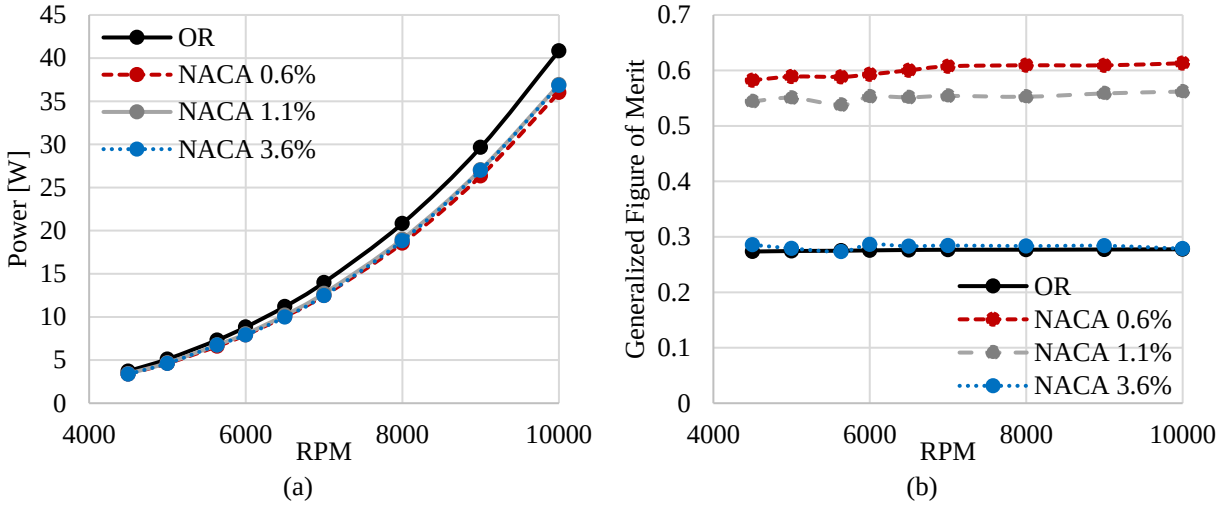

Fig. 18 Comparison of (a) total power and (b) generalized Figure of Merit FM^* for Gemfan 5152 Flash propeller with NACA-based shroud design (NACA) against open rotor (OR) configuration. The NACA shrouds include different tip clearances of 0.6%, 1.1%, and 3.6%.

To understand the factors for the performance gains in shrouded designs, we can explore the underlying flow behaviors for the different configurations. Fig. 19 shows examples of the simulation results for the different configurations at 5,635 RPM. The velocity field in Fig. 19 (a-b) and corresponding streamlines in (c-d) illustrate how the shroud guides the flow to align parallel to the propeller axis of rotation before reaching the propeller. This explains the improved aerodynamic performance of shrouded configurations. The results also illustrate a smooth transition of the NACA-shaped shroud which further explains the improved performance of the cambered shroud designs. For the open rotor we can observe how the jets created behind the rotor mix much faster leading to larger dissipation and hence less propulsive thrust in this configuration. The examples of flow results shown here demonstrate the advantages of using a simulation-based design approach in addition to experimental studies in the design of ducted propulsion systems for multirotor vehicles.

Finally, comparison between experimental findings in Fig. 9 and the corresponding CFD results in Fig. 17 shows that both methods can predict the performance gains in shrouded designs. However, the improvements appear much more dominant in experiments with 250% increase in thrust compared to the 160% increase in the CFD results comparing open rotor and shrouded configurations. The experimental results also predict lower overall thrust values for the both configurations compared to the CFD results. While the CFD studies consider a clean configuration with no blockage, we can observe from Fig. 4 that the experimental setup in this work experiences significant blockage due to the thrust stand, shroud mounting and anemometer interfering with the propeller wake. As experimentally shown in [20], a blockage of 64% of the propeller disk can reduce the resulting thrust coefficient by 60% for low advance ratios. This reduction in thrust while exhibiting a minimal effect on power, is consistent with the results shown in this work. The results can be improved if larger propeller diameters are considered for the comparison where the blockage effects are less dominant. The study therefore shows that a balanced analysis using CFD in addition to a rapid design approach using 3D printing is ideal for the design of shrouded multirotor configurations.

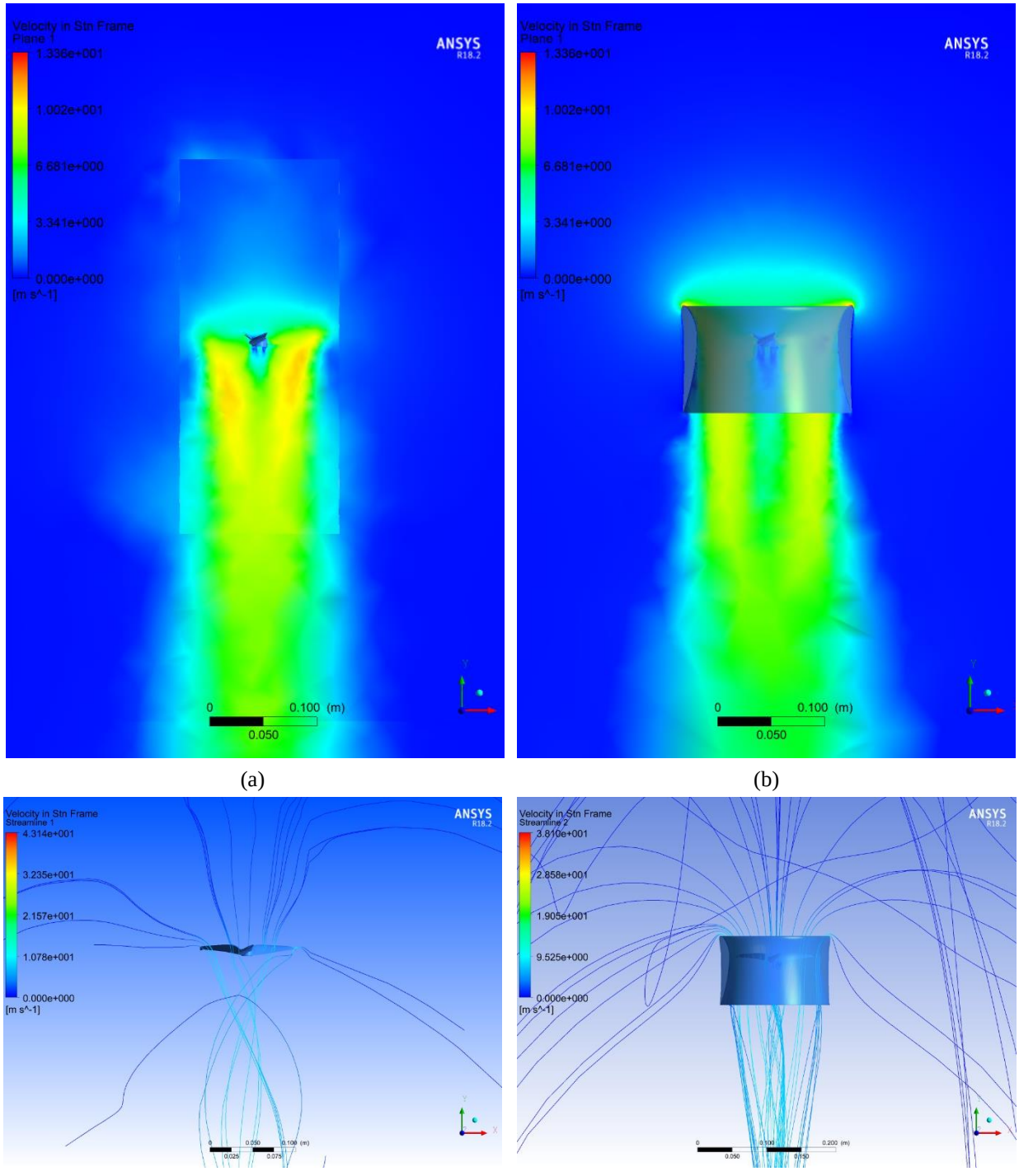

Fig. 19 Comparison of (a-b) velocity in stationary frame and (c-d) velocity streamlines for open rotor and shrouded design at 5,635 RPM.

V. Conclusion

The increasing trend of multirotor UAV operation in urban environments calls for additional safety measures to address the danger of rotating propellers interacting with objects and people in the vehicle vicinity. Novel designs therefore feature propeller guards and shrouds to encapsulate the propeller and protect the surrounding. Such rotor shrouds have been historically also used to increase the rotor performance. However, the performance of shrouded rotors depends heavily on the shroud geometry. This work therefore proposes a novel approach for the rapid design of unconventional rotor shrouds combining a rapid manufacturing approach with a high-fidelity CFD prediction tool. Using 3D printing we designed different propeller shrouds to experimentally investigate the performance gains of unconventional shroud geometries using NACA-shaped profiles. The experimental approach is complimented with simulation-based studies of the same shroud and propeller geometries. The presented studies provide insights into the flow features of novel shroud configurations. Comparison between experimental and simulation results for a 5-inch, 3-bladed propeller indicate that the experimental system tends to underpredict the resulting thrust, and hence resulting Figure of Merit for both open rotor and shrouded configurations. This drop in thrust output is likely attributed to blockage effects since the relatively small propeller is significantly blocked by the thrust stand and other sensors. Hence, if the approach is extended to larger configurations, we would expect better comparison between simulation and experimental similar to the validation cases considered in this work. Finally, the proposed approach can be extended to co-axial configurations which would be relevant to the latest eVTOL designs and heavy-lift UAVs.

Appendix

Table 6 CFD results for Gemfan 5152 Open Propeller,

RPM	Rev/s	Rad/s	Thrust (N)	Moment (Nm)	Power (W)	CFD	
						C_T	C_T
4500	75.00	471.24	0.40	7.89E-03	3.72	0.22	0.22
5000	83.33	523.60	0.50	9.75E-03	5.11	0.22	0.22
5635	93.92	590.10	0.63	1.24E-02	7.32	0.22	0.22
6000	100.00	628.32	0.72	1.40E-02	8.83	0.22	0.22
6500	108.33	680.68	0.84	1.65E-02	11.20	0.22	0.22
7000	116.67	733.04	0.98	1.91E-02	14.00	0.23	0.22
8000	133.33	837.76	1.27	2.49E-02	20.82	0.22	0.22
9000	150.00	942.48	1.61	3.15E-02	29.65	0.22	0.22
10000	166.67	1047.20	2.00	3.90E-02	40.84	0.23	0.22

Table 7 CFD results for Gemfan 5152 Shrouded Propeller 0.78 mm Tip Clearance 0.6%.

RPM	Propeller			Shroud			Total			CFD	
	Thrust (N)	Moment (Nm)	Power (W)	Thrust (N)	Moment (Nm)	Power (W)	Thrust (N)	Moment (Nm)	Power (W)	C_T	C_P
4500	0.33	0.01	3.31	0.31	1.67E-04	0.08	0.64	0.01	3.39	0.36	0.20
5000	0.40	0.01	4.52	0.39	1.83E-04	0.10	0.79	0.01	4.62	0.36	0.20
5635	0.51	0.01	6.47	0.49	2.21E-04	0.13	1.00	0.01	6.60	0.36	0.20
6000	0.58	0.01	7.76	0.56	2.50E-04	0.16	1.14	0.01	7.92	0.36	0.20
6500	0.68	0.01	9.88	0.66	2.42E-04	0.16	1.35	0.01	10.04	0.36	0.20
7000	0.79	0.02	12.29	0.78	2.67E-04	0.20	1.57	0.02	12.49	0.36	0.19
8000	1.03	0.02	18.31	1.02	2.89E-04	0.24	2.05	0.02	18.55	0.36	0.19
9000	1.30	0.03	25.99	1.28	3.62E-04	0.34	2.58	0.03	26.33	0.36	0.19
10000	1.61	0.03	35.58	1.59	4.12E-04	0.43	3.20	0.03	36.01	0.36	0.19

Table 8 CFD results for Gemfan 5152 Shrouded Propeller 1.42 mm Tip Clearance 1.11%.

RPM	Propeller			Shroud			Total			CFD	
	Thrust (N)	Moment (Nm)	Power (W)	Thrust (N)	Moment (Nm)	Power (W)	Thrust (N)	Moment (Nm)	Power (W)	C_T	C_P
4500	0.34	0.01	3.34	0.28	1.79E-04	0.08	0.62	0.01	3.43	0.35	0.20
5000	0.41	0.01	4.57	0.35	2.07E-04	0.11	0.77	0.01	4.68	0.35	0.20
5635	0.53	0.01	6.57	0.43	3.11E-04	0.18	0.97	0.01	6.76	0.34	0.20
6000	0.59	0.01	7.85	0.51	2.98E-04	0.19	1.11	0.01	8.03	0.35	0.20
6500	0.70	0.01	9.97	0.59	3.43E-04	0.23	1.29	0.01	10.20	0.35	0.20
7000	0.81	0.02	12.46	0.69	3.79E-04	0.28	1.50	0.02	12.73	0.35	0.20
8000	1.07	0.02	18.57	0.90	5.37E-04	0.45	1.96	0.02	19.02	0.35	0.20
9000	1.35	0.03	26.41	1.15	6.94E-04	0.65	2.50	0.03	27.06	0.35	0.20
10000	1.66	0.03	36.07	1.43	8.11E-04	0.85	3.09	0.04	36.92	0.35	0.20

Table 9 CFD results for Gemfan 5152 Shrouded Propeller 4.54 mm Tip Clearance 3.6%.

RPM	Propeller			Shroud			Total			CFD	
	Thrust (N)	Moment (Nm)	Power (W)	Thrust (N)	Moment (Nm)	Power (W)	Thrust (N)	Moment (Nm)	Power (W)	C_T	C_P
4500	0.33	0.01	3.23	0.08	3.06E-04	0.14	0.41	0.01	3.37	0.23	0.20
5000	0.41	0.01	4.43	0.08	3.36E-04	0.18	0.50	0.01	4.61	0.23	0.20
5635	0.55	0.01	6.67	0.08	1.05E-04	0.06	0.63	0.01	6.73	0.23	0.20
6000	0.60	0.01	7.64	0.13	4.23E-04	0.27	0.73	0.01	7.91	0.23	0.20
6500	0.70	0.01	9.65	0.14	4.84E-04	0.33	0.84	0.01	9.98	0.23	0.19
7000	0.81	0.02	12.08	0.17	5.27E-04	0.39	0.98	0.02	12.47	0.23	0.19
8000	1.09	0.02	18.39	0.20	5.35E-04	0.45	1.29	0.02	18.84	0.23	0.20
9000	1.40	0.03	26.47	0.24	5.46E-04	0.51	1.64	0.03	26.99	0.23	0.20
10000	1.73	0.03	36.29	0.27	5.25E-04	0.55	1.99	0.04	36.84	0.23	0.20

References

[1] D. Moormann, "DHL Parcelcopter research flight campaign 2014 for emergency delivery of medication," in *ICAO RPAS Symposium*, Montreal, 24 March 2015.

[2] S. Yilmaz, D. Erdem and M. Kavsaoglu, "Performance of a ducted propeller designed for UAV applications at zero angle of attack flight: An experimental study," *Aerospace Science and Technology*, vol. 45, pp. 376-386, 2015.

[3] D. Cheng, A. C. Charles, S. Srigrarom and H. Hesse, "Morphing Concept for Multirotor UAVs Enabling Stability Augmentation and Multiple-Parcel Delivery," in *AIAA SciTech Forum*, San Diego, CA, USA, 2019.

[4] W. Ong, S. Srigrarom and H. Hesse, "Design Methodology for Heavy-Lift Unmanned Aerial Vehicles with Coaxial Rotors," in *AIAA Scitech Forum*, San Diego, CA, USA, 2019.

[5] R. T. Taylor, "Experimental investigation of the effects of some shroud desgin variables on the static thrust characteristics of a small-scale shrouded propeller submerged in a wing," National Advisory Committee For Aeronautics (NACA) , Washington, 1958.

[6] A. H. Sacks and J. A. Burnell, "Ducted propellers - A critical review of the state of the art," *Progress in Aerospace Sciences*, vol. 3, pp. 85-135, 1962.

[7] J. L. Pereira, "Hover and wind-tunnel testing of shrouded rotors for improved micro air vehicle design," Ph.D. Thesis, University of Maryland, College Park, MD, USA, 2008.

[8] J. L. Pereira and I. Chopra, "Hover Tests of Micro Aerial Vehicle-Scale Shrouded Rotors, Part II: Flow Field Measurements," *Journal of the American Helicopter Society*, vol. 54, p. 12002–1200226, 2009.

[9] V. Hrishikeshavan, J. Black and I. Chopra, "Design and Performance of a Quad-Shrouded Rotor Micro Air Vehicle," *Journal of Aircraft*, vol. 551, no. 3, pp. 779-791, 2014.

[10] P. Martin and C. Tung, "Performance and Flowfield Measurements on a 10-inch Ducted Rotor VTOL UAV," NASA Technical Report, Ames Research Center, 2004.

[11] J. Ahn and K. Lee, "Performance Prediction and Design of a Ducted Fan System," in *40th AIAA/ASME/SAE/ASEE Joint Propulsion Conference and Exhibit*, Fort Lauderdale, Florida, 2004.

[12] H. A. Kutty and P. Rajendran, "3D CFD Simulation and Experimental Validation of Small APC Slow Flyer Propeller Blade," Aerospace Volume 4 Issue 10, Malaysia, Penang, 2017.

[13] E. Kuantama and R. Tarca, "Quadcopter thrust optimization with ducted-propeller," *MATEC Web of Conferences*, vol. 126, 2017.

[14] C. Xu, "CFD Investigation into Propeller Spacing and Pitch Angle for a Ducted Twin Counter Rotating Propeller System," Masters Thesis, RMIT University, Australia, 2015.

[15] D. Cheng, W. Ong, A. C. Charles, B. Hum, N. Ho, G. E. Hogan, J. Tan, I. Ibrahim, H. Hesse and S. Srigrarom, "Development of a VTOL Flying Car Concept," in *14th International Conference on Intelligent Unmanned System*, Jeju, South Korea, 2018.

[16] RC Benchmark, "Series 1580 - Thrust Stand and Dynamometer," [Online]. Available: https://www.rcbenchmark.com/dynamometer-series-1580/..

[17] ANSYS, "FLUENT 12.0 Theory Guide - 2.3.1 The Multiplie Reference Frame Model," ANSYS, Inc., 2009.

[18] J. Brandt and M. Selig, "Propeller Performance Data at Low Reynolds Numbers," vol. 49th AIAA Aerospace Sciences Meeting, pp. AIAA Paper 2011-1255, 2011.

[19] T. Koronowicz, Z. Krzemianowski, T. Tuszkowska and J. A. Szantyr, "A complete design of ducted propellers using the new computer system," *Polish Maritime Research*, vol. 2, pp. 34-39, 2009.

[20] R. MacNeill and D. Verstraete, "The Effects of Blockage on the Performance of Small Propellers," in *20th Australasian Fluid Mechanics Conference*, Perth, Australia, 2016.